Journal of the Ceramic Society of Japan 102 [8] 737-741 (1994)

Paper

Crystal Structure and Ionic Conductivity of a Layered Perovskite, $Na_2La_2Ti_3O_{10}$

Kenji TODA, Yutaka KAMEO*, Masayuki FUJIMOTO** and Mineo SATO*

Department of Active Material Chemistry, Graduate School of Science and Technology, Niigata University, 8050, Ikarashi 2-no-cho, Niigata-shi 950-21
**Department of Chemistry and Chemical Engineering, Faculty of Engineering, Niigata University, 8050, Ikarashi 2-no-cho, Niigata-shi 950-21*
***Taiyo Yuden Co., Ltd., 562, Hongo-Tsukanaka, Haruna-machi, Gunma 370-33*

層状ペロブスカイト $Na_2La_2Ti_3O_{10}$ の構造解析とイオン伝導性

戸田健司・亀尾 裕*・藤本正之**・佐藤峰夫*

新潟大学大学院自然科学研究科，950-21 新潟市五十嵐二の町 8050
*新潟大学工学部化学システム工学科，950-21 新潟市五十嵐二の町 8050
**太陽誘電(株)，370-33 群馬県榛名町本郷塚中 562

[Received February 14, 1994; Accepted May 19, 1994]

An ion-exchangeable layered perovskite compound, $Na_2La_2Ti_3O_{10}$, was directly synthesized by a solid-state reaction. The crystal structure of $Na_2La_2Ti_3O_{10}$ was determined by electron diffraction analysis and Rietveld analysis for the powder X-ray diffraction pattern. The unit cell is tetragonal with $a=0.383528(7)$ nm, $c=2.85737(7)$ nm and $Z=2$ with the space group $I4/mmm$ (No. 139). The structure of this compound is analogous to that of the Ruddlesden-Popper phases. The ionic conductivity of $Na_2La_2Ti_3O_{10}$ was not very high compared with those of niobate compounds, $NaLaNb_2O_7$ and $NaCa_2NaNb_4O_{13}$. Such a low ionic conductivity is due to the rigid rock-salt-type coordination around sodium ions located at the interlayer.

Key-words : *Rietveld analysis, Ionic conductivity, Layered perovskite, Sodium lanthanum titanate*

1. Introduction

Ion-exchangeable layered perovskites made up of NbO_6 or TiO_6 octahedra have gained interest in recent years, not only because of their excellent ion-exchange ability but also their intercalation reactions[1)-10)] and photocatalytic reactions.[11)]

The synthesis of $M_2La_2Ti_3O_{10}$ (M=Li, Na, K) has been reported for the first time by Vallino.[12)] Recently ion-exchange reactions of $M_2Ln_2Ti_3O_{10}$ (M=Na, K, Rb; Ln=rare earth ions) have been found independently by Gondrand and Joubert,[3)] and Gopalakrishnan and Bhat.[4)] However, the crystal structure of $M_2Ln_2Ti_3O_{10}$ remains unknown although prototype structure models are presumed on the basis of lattice constants and on the indexing of the powder X-ray diffraction patterns. Although many of the ion-exchangeable compounds containing sodium ions, for example, Na-β-alumina, exhibit high ionic conductivity, there are few studies on ionic conductivity of interlayer ions for layered perovskites consisting of TiO_6.

In our previous study,[6)] we have clarified the silver ionic conductive properties of a silver-exchanged compound $Ag_2La_2Ti_3O_{10}$, which crystallizes into a Ruddlesden-Popper structure and exhibits a relatively strong covalent character for the Ag-O bond along the direction perpendicular to the perovskite layer. It shows mixed conduction with silver ions and electrons above 200℃. On the other hand, the main structure of $AgLaNb_2O_7$ which shows almost pure ionic conduction is also analogous to that of the Ruddlesden-Popper phase but the environment around the interlayer ions in this compound is somewhat different, i.e., silver ions are located on the nearly tetrahedral site with 50% occupancy in the interlayer.[7)] These structural differences between titanates and niobates are thought to be reflected by their conductive behaviors. This is because the TiO_6 and NbO_6 octahedra exhibit the different interactions between the perovskite sheets and the interlayer ions due to the different oxidation states of their central cations.[8)] It is expected that $Na_2La_2Ti_3O_{10}$ also shows pure ionic conduction. Therefore, we can give a clear discussion for the mechanism of ionic conductive behavior in the layered perovskite compounds.

In this paper, the structure and ionic conductivity of $Na_2La_2Ti_3O_{10}$ are investigated and compared with those of niobate compounds[9)] such as $NaLaNb_2O_7$ and $NaCa_2NaNb_4O_{13}$, since these two compounds in which interlayer ion environment is different from that of the Ruddlesden-Popper phase also show pure ionic conduction. Based on the comparison between titanate and niobate compounds, we have discussed the mechanism of ionic conductive behavior in layered perovskite compounds.

2. Experimental

$Na_2La_2Ti_3O_{10}$ was prepared by a solid-state reaction. The starting materials were Na_2CO_3, La_2O_3 and

TiO_2. An excess amount of Na_2CO_3 (30 mol%) was added to compensate for loss due to the evaporation of sodium component. The reactants were ground, pelletized and then fired in an open alumina crucible. The following three stages for the calcination were adopted in order to obtain a single phase. The mixture was fired at 550℃ for 12h in air, subsequently heated at 1000–1100℃ for another 6h in O_2 flow, and finally cooled slowly (<3℃$\cdot min^{-1}$) to room temperature. After the reaction, the product was washed with distilled water and dried at 100℃ for 24h.

Thermogravimetric analysis (TGA) and differential thermal analysis (DTA) were carried out using a Mac Science thermal analyzer system 001 at a heating rate of 5℃$\cdot min^{-1}$ in air.

Thin specimens for electron microscopic analysis were obtained by crushing and mounting the crystal fragments on a Cu grid. Electron microscopic analysis was carried out with an ABT (Topcon) EM002B electron microscope operating at 200 kV. Chemical analysis was carried out by the EDX method using an electron microscope fitted with an EDX analyzer.

Powder X-ray diffraction patterns were recorded on a Rigaku RAD-rA diffractometer, using Cu Kα radiation which was monochromatized by a curved crystal of graphite. The data were collected in a step-scanning mode in the 2θ range of 5–100° with a step width of 0.02° and a step time of 4s. Data analysis was carried out by the Rietveld method, using the RIETAN profile refinement program[13] on an ACOS2010 computer at Niigata University.

Ionic conductivity of $Na_2La_2Ti_3O_{10}$ was measured on a pressed pellet by a complex impedance technique between 40 Hz and 100 kHz using a Hioki 3520 Hi Tester in the temperature range of 300–800℃.

3. Results and discussion

In order to obtain a monophasic $Na_2La_2Ti_3O_{10}$ compound, we first used the same method as that reported by Gondrand and Joubert.[3] However, the monophasic compound could not be obtained by their preparation conditions. The impurity phases of $La_{2/3}TiO_{3-x}$[14] and $NaLaTiO_4$[15] were always observed in the reaction product. After some trial and error, the preparation conditions consisting of the three steps as mentioned in the experimental section are found to be the best for the preparation of a single-phase product. In the absence of the first step, the end product is a defective perovskite, $La_{2/3}TiO_{3-x}$. The defective perovskite is considered to be more thermodynamically stable than the layered perovskite, $Na_2La_2Ti_3O_{10}$, around this temperature range. It was found that the presence of the intermediate product, $La_2O_2CO_3$, is necessary to prevent the formation of $La_{2/3}TiO_{3-x}$ in the reaction. The reaction temperature for the first step should not be permitted to exceed 600℃, because the defective perovskite is preferentially formed over this temperature. It is necessary to keep the reaction temperature for the second step within the range from 1000 to 1100℃, since the impurity phase, $NaLaTiO_4$, is produced rather than $Na_2La_2Ti_3O_{10}$ below this temperature range.

Thermogravimetric analysis indicated that $Na_2La_2Ti_3O_{10}$ does not take any hydrous form even though the compound was washed with distilled water. This result is in contrast to that of the corresponding potassium compound, $K_2La_2Ti_3O_{10}$,[4),6)] which contains 1.7 water molecules in the interlayer. Contrary to the titanate compounds, $NaLaNb_2O_7$ has 1.6 water molecules in the interlayer and $KLaNb_2O_7$ does not take any hydrous form.[8),10)] $KLaNb_2O_7$ forms a base-centered lattice wherein potassium ions have trigonal prismatic coordination, while $NaLaNb_2O_7$ takes a body-centered lattice wherein sodium ions have almost regular tetrahedral coordinations. Therefore, the differences of the hydration behavior are due to the differences of interlayer space and not nature of interlayer cation. Since the crystal structure of $Na_2La_2Ti_3O_{10}$ and $K_2La_2Ti_3O_{10}$ are exactly the same as shown later, the hydration behavior of these compounds can be understood on the basis of the Coulomb interaction between the interlayer ions and perovskite layer. The Coulomb attractive interaction is much stronger for the sodium compound than for the of potassium compound because of the smaller ionic radius of Na^+ ions. Therefore, in the sodium compound, the energetic gains obtained by hydration of Na^+ ions do not exceed the energy required to expand the interlayer space.

Figure 1 shows a selected electron diffraction pattern of $Na_2La_2Ti_3O_{10}$. The indexing for each spot could be successfully accomplished in the light of analogy with the crystal structure of $Sr_4Ti_3O_{10}$,[16] one of the members of Ruddlesden–Popper phases with a tetragonal system. It was found that the incident electron beam runs along the $[\bar{1}11]$ direction and that the spots were indexed as shown in Fig. 1. Approximate cell parameters estimated from the

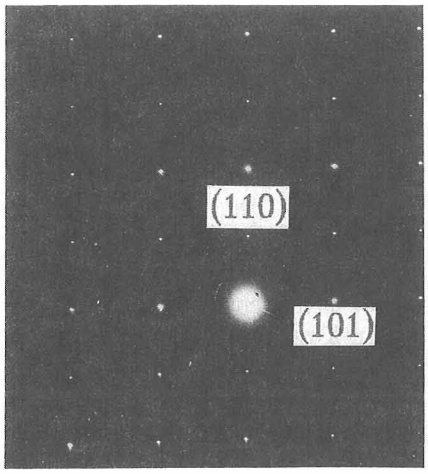

Fig. 1. Electron diffraction pattern of $Na_2La_2Ti_3O_{10}$.

diffraction pattern are $a=0.38$ nm and $c=2.8$ nm, and the reflection condition is $h+k+l=2n$ for (hkl) reflections. It is obvious that the doubling of the a-axis as reported by Gondrand and Joubert[3] is not observed in our result. There are two possible explanations for this disagreement. As mentioned above, the synthesis of the single-phase $Na_2La_2Ti_3O_{10}$ is achieved only under the severely controlled preparation conditions particularly in the case of heating temperatures. Therefore, we suppose that some impurities may be present in their sample. In addition, the cooling rate after the high-temperature reaction may lead to some distortions of the crystal structure. Since there are no data of electron diffraction patterns and cooling rate in their paper, we do not discuss this in detail here. Figure 2 shows the electron micrograph of $Na_2La_2Ti_3O_{10}$ with $[\bar{1}11]$ incidence corresponding to the same zone as that of the electron diffraction pattern in Fig. 1. Two kinds of streaks which intersect each other with an angle nearly equal to 90° can be seen. One has a d-spacing of 0.28 nm corresponding to that of the [110] direction, and the other a d-spacing of 0.38 nm corresponding to that of the [101] direction. These distances coincide well with those for the edge and diagonal of a TiO_6 octahedron found in some titanates.

Indexing of the powder X-ray diffraction patterns obtained was examined with the aid of the computer program CELL[17] on the basis of tetragonal symmetry. The possible space groups were chosen from the results. The reflection condition found was $h+k+l=2n$ for hkl reflections, which was consistent with the result for the electron diffraction. This condition leads to eight possible space groups, $I\bar{4}$, $I4/m$, $I422$, $I4mm$, $I\bar{4}m2$, $I\bar{4}2m$ and $I4/mmm$.

The Rietveld refinement was carried out for all of the space groups in the early refinement stages. The reflection peak observed at $2\theta=6.1°$ in the powder diffraction pattern was found to deviate greatly from the calculated peak profile due to an asymmetric effect of peak shape at such low 2θ region. Therefore, this reflection peak was eliminated from the Rietveld refinement. Finally, the $I4/mmm$ space group gives the most satisfactory fitting to the powder X-ray diffraction pattern. The final reliability factors achieved were $R_{wp}=12.87\%$, $R_p=9.86\%$, $R_I=3.83\%$, $R_F=2.14\%$. The results of the pattern fitting are shown in Fig. 3 and the crystallographic data are listed in Table 1. The positional parameters and the selected interatomic distances and angles are listed in Table 2 and Table 3, respectively.

The values of isotropic thermal parameters are highly scattered. In particular, the value for O(1) is considerably large, and some of values for other sites must be fixed to a positive value because of their con-

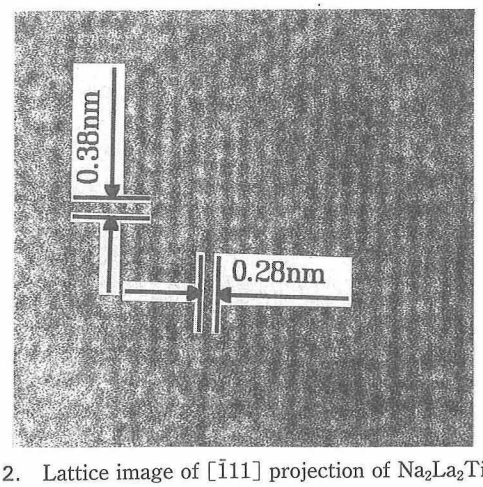

Fig. 2. Lattice image of $[\bar{1}11]$ projection of $Na_2La_2Ti_3O_{10}$.

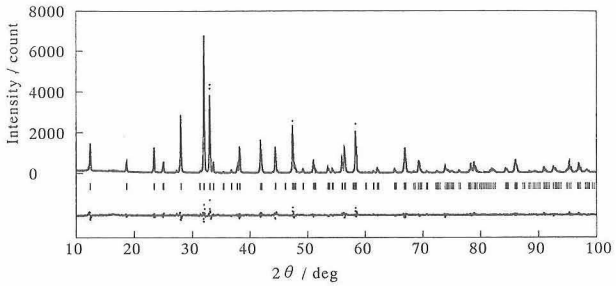

Fig. 3. Powder XRD pattern fitting for $Na_2La_2Ti_3O_{10}$. The calculated and observed patterns are represented by the top solid line and dots, respectively. The vertical marks in the middle show positions calculated for Bragg reflections. The trace on the bottom is a plot of the difference between calculated and observed intensities.

Table 1. Crystallographic Data of $Na_2La_2Ti_3O_{10}$

Radiation	CuK α
2 θ range (°)	5-100
Step scan increment (2 θ)	0.04
Count time (s · step^{-1})	4
Space group	I4/mmm
a (nm)	0.383528(7)
c (nm)	2.85737(7)
Volume (nm^3)	0.420301
Z	2
Calculated density (g · cm^{-3})	4.958
No. of reflections	195
No. of refined parameters	26
Reliable factors	$R_{wp}=0.1287$, $R_p=0.0986$ $R_I=0.0383$, $R_F=0.0214$

Table 2. Positional Parameters of $Na_2La_2Ti_3O_{10}$

Atom	Site[a)]	g[b)]	x	y	z	B / nm^2
Na	4e	1.0	0.0	0.0	0.2895(9)	0.005
La	4e	1.0	0.0	0.0	0.4246(1)	0.0006(11)
Ti(1)	2a	1.0	0.0	0.0	0.0	0.001
Ti(2)	4e	1.0	0.0	0.0	0.1491(4)	0.001
O(1)	4c	1.0	0.0	0.5	0.0	0.080(20)
O(2)	4e	1.0	0.0	0.0	0.065(1)	0.005
O(3)	8g	1.0	0.0	0.5	0.137(1)	0.004(6)
O(4)	4e	1.0	0.0	0.0	0.210(1)	0.008(8)

a) Multiplicity and Wyckoff notation.
b) Occupancy.

Table 3. Bond Distances (nm) and Angles (°) of $Na_2La_2Ti_3O_{10}$

Distance		Angle	
Na - O(4)	0.2278(43)	O(2) - Ti(2) - O(3)	79.4(8)x4
Na - O(4)$^{i)}$	0.27120(4)x4	O(4) - Na - O(4)	90.2(5)x4
Na - O(3)$^{i)}$	0.2854(28)x4		
La - O(1)$^{i)}$	0.2884(3)x4		
La - O(2)$^{i)}$	0.2729(4)		
La - O(3)$^{i)}$	0.2594(19)		
Ti(1) - O(1)	0.1918(0)x4		
Ti(1) - O(2)	0.1848(35)x2		
Ti(2) - O(2)	0.2412(37)		
Ti(2) - O(3)	0.1951(5)x4		
Ti(2) - O(4)	0.1734(38)	Symmetry code	
O(1) - O(1)$^{ii)}$	0.2712(0)x4		
O(1) - O(2)	0.2663(24)x4	None x, y, z	
O(2) - O(3)	0.2809(32)x4	i) 1/2-x, 1/2-y, 1/2-z	
O(3) - O(3)$^{ii)}$	0.2712(0)x4	ii) -y, x, z	
O(3) - O(4)	0.2839(36)x4		

version to negative values without fixing. This may be due to an insufficient correction for the preferred orientation because the prepared sample exhibits an extremely large cleavage perpendicular to the *c*-axis. Another origin for the scattered isotropic thermal parameters is possible, i.e., the existence of intergrowth. There have been many studies on the intergrowth of titanate compounds.[18)-20)] However, this phenomenon is very troublesome and has not yet been clarified theoretically. The information of short-range disorder of the crystal structure cannot be obtained by powder X-ray diffraction pattern analysis. Another approach, for example, high-resolution electron microscopic study, is necessary to determine intergrowth occurs in this material.

The crystal structure of $Na_2La_2Ti_3O_{10}$ is illustrated in Fig. 4. The structure is composed of a perovskite unit with three layers and a rock-salt-type unit (NaO) stacked alternately along the *c*-axis. The adjacent triple perovskite sheets, $La_2Ti_3O_{10}$, are stacked with a displacement by 1/2 along the (110) direction. A sodium ion in this compound occupies the nine-fold sites between the two perovskite layers. A lanthanum ion occupies the twelve-fold sites in the center of the perovskite lattice. The feature of the crystal structure in this compound is the same as those of proton, potassium and silver compounds.[4),6)] The relative arrangement of the adjacent perovskite sheets is independent of its ionic size while existing in the interlayer. This stacking feature is in contrast to that of niobate compounds.[10)] In niobate oxides with a layered perovskite structure, only one sodium ion can be accommodated in the interlayer space per NbO_6 octahedron located toward the space. No matter how many perovskite layers are constructed, such $NaLaNb_2O_7$, $NaCa_2Nb_3O_{10}$, and $NaCa_2NaNb_4O_{13}$, this is always true due to the high positive charge of the central ion of the NbO_6 octahedron. This situation can lead to a lower charge density state for the interlayer space. As the result, the Coulomb interaction between the perovskite layer and the interlayer ion is relatively weak, reflecting a variety of stacking features of the adjacent perovskite layer blocks owing to the ionic size of the interlayer ions. On the other hand, in titanate oxides, the lower charge of the central ion of the TiO_6 octahedron is compensated by two interlayer monovalent ions per TiO_6 octahedron located toward the interlayer, i.e., a high positive charge density state is realized in the interlayer space. This is consistent with the fact that $Na_2La_2Ti_3O_{10}$ crystal is stable upon the irradiation of a high-energy electron beam in the electron microscopy studies.

Figure 5 shows the environment of titanium atoms in $Na_2La_2Ti_3O_{10}$. A large distortion of the TiO_6 octahedra exists in the structure. The TiO_6 octahedron located inside of the perovskite layers is close to an ideal octahedron, while those located outside of the layer are fairly distorted. The oxygen with a fairly shortened distance of Ti–O is located toward sodium ions between the triple perovskite layers. These bond characters are similar to those of $NaLaNb_2O_7$.[8)] The distortion of metal-oxygen octahedra in the perovskite layer is a quite common feature observed in layered perovskites which exhibit an ion-exchange property.[6),8)] Such shortness of the Ti–O distance

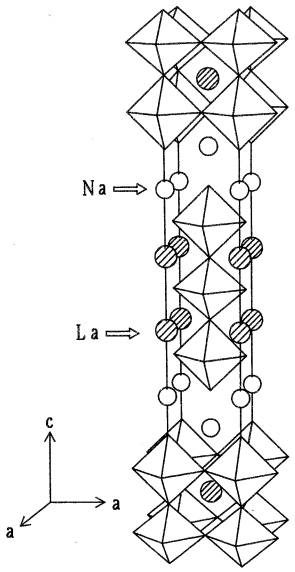

Fig. 4. Crystal structure of $Na_2La_2Ti_3O_{10}$. The octahedra are TiO_6 units.

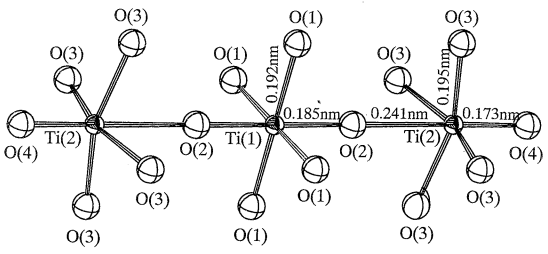

Fig. 5. Environment around titanium atoms in the perovskite layer of $Na_2La_2Ti_3O_{10}$.

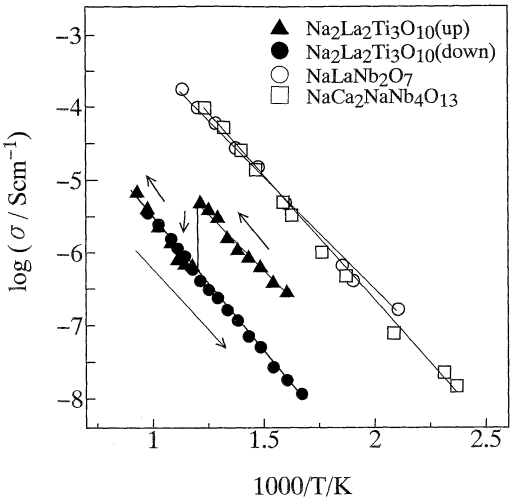

Fig. 6. Temperature dependence of ionic conductivity of $Na_2La_2Ti_3O_{10}$, $NaLaNb_2O_7$ and $NaCa_2NaNb_4O_{13}$. (▲) represents data for temperature increasing direction and (●) for temperature decreasing direction.

seems to cause less interaction between the sodium and the crystal lattice of the sheets. Therefore, it is possible in this situation to exchange the ions in the interlayer with other alkali ions and protons as reported previously.[3),4),6)]

Figure 6 shows the ionic conductivity of $Na_2La_2Ti_3O_{10}$ as a function of temperature. A sharp drop of ionic conductivity was observed at around 575°C. Since the X-ray powder pattern above this temperature showed the formation of the defective perovskite, $La_{2/3}TiO_{3-x}$, in this sample, this change is due to the decomposition of $Na_2La_2Ti_3O_{10}$. It is interesting to compare the ionic conductivity of $Na_2La_2Ti_3O_{10}$ with those of niobate compounds. The value of ionic conductivity of $Na_2La_2Ti_3O_{10}$ is approximately 10 times less than those of niobate compounds, $NaLaNb_2O_7$ and $NaCa_2NaNb_4O_{13}$.[9)] These results are analogous to those obtained using the silver-exchange compounds.[6)] Such difference in the ionic conductivity between the titanate and the niobate compounds is due to the difference in the charge density of the interlayer contributed by the central ions (Ti^{4+} and Nb^{5+}) of the TiO_6 and NbO_6 octahedra. The common features among sodium and silver compounds are due to the similarity of their crystal structure. The high charge density in the interlayer of titanate compounds leads to strong electrostatic interaction between the perovskite layer. The environment of the sodium atoms in $Na_2La_2Ti_3O_{10}$ is illustrated in Fig. 7. Here, sodium ions are situated in a rigid rock-salt-type coordination with 100% occupancy. On the other hand, sodium ions in $NaLaNb_2O_7$ and $NaCa_2NaNb_4O_{13}$ are located in a tetrahedral coordination with 50% occupancy. Therefore, the ionic motion in $Na_2La_2Ti_3O_{10}$ is more tightly restricted than those of $NaLaNb_2O_7$ and $NaCa_2NaNb_4O_{13}$. The differences of coordination around sodium ion reflect the differences of ionic conductivity between the titanate and niobate compounds. These results indicate that the ion conducting behavior in the layered perovskite compounds is mainly dependent upon the environment around the conductive ions in the interlayer.[9)]

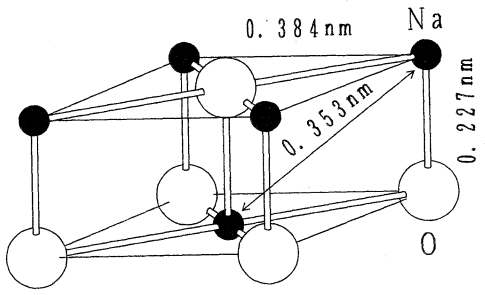

Fig. 7. Environment around sodium atoms in $Na_2La_2Ti_3O_{10}$.

Acknowledgements We are indebted to Mr. K. Uematsu for his help in the preparation of samples, to Mr. H. Minagawa for his help in data collection of X-ray powder diffraction measurements and to Dr. Y. Kitayama for her help in DTA and TGA measurements.

References

1) M. Dion, M. Ganne and M. Tournoux, *Mater. Res. Bull.*, 16, 1429–35 (1981).
2) A. J. Jacobson, J. T. Lewandowski and J. W. Johnson, *J. Less-Common Metals*, 116, 137–46 (1986).
3) M. Gondrand and J. C. Joubert, *Rev. Chim. Miner.*, 24, 33–41 (1987).
4) J. Gopalakrishnan and V. Bhat, *Inorg. Chem.*, 26, 4299–301 (1987).
5) G. Okada, S. Ohmiya, S. Matsushima and K. Kobayashi, *Denki Kagaku*, 60, 336–38 (1992).
6) M. Sato, K. Toda, J. Watanabe and K.Uematsu, *Nippon Kagaku Kaishi*, 640–46 (1993).
7) M. Sato, J. Watanabe and K. Uematsu, *J. Solid State Chem.*, 107, 460–70 (1993).
8) M. Sato, J. Abo and T. Jin, *Solid State Ionics*, 57, 285–93 (1992).
9) M. Sato, Y. Kono and T. Jin, *J. Ceram. Soc. Japan*, 101, 980–84 (1993).
10) M. Sato, J. Abo, T. Jin and M. Ohta, *J. Alloys Comp.*, 192, 81–83 (1993).
11) K. Domen, J. Yoshimura, T. Sekine, A. Tanaka and T. Onishi, *Cat. Lett.*, 4, 339–44 (1990).
12) M. Vallino, *Atti Accad. Sci. Torino, Cl. Sci. Fis., Mat. Nat.*, 117, 85–89 (1985).
13) F. Izumi, *Nippon Kesshou Gakkaishi*, 27, 23–31 (1985).
14) M. Abe and K. Uchino, *Mater. Res. Bull.*, 9, 147–56 (1974).
15) G. Blasse, *J. Inorg. Nucl. Chem.*, 30, 656–58 (1968).
16) S. N. Ruddlesden and P. Popper, *Acta Cryst.*, 11, 54–55 (1958).
17) Y. Takaki, T. Taniguchi, H. Yamaguchi and T. Ogura, *Yogyo-Kyokai-Shi*, 95, 610–15 (1987).
18) R. J. D. Tilley, *J. Solid State Chem.*, 21, 293–301 (1977).
19) K. R. Udayakumar and A. N. Cormack, *J. Am. Ceram. Soc.*, 71, 469–71 (1988).
20) M. Fujimoto, J. Tanaka and S. Shirasaki, *Jpn. J. Appl. Phys.*, 27, 1162–66 (1988).